Rapid Communication

On the origin of the toughness of mineralized tissue: microcracking or crack bridging?

R.K. Nalla, J.J. Kruzic, and R.O. Ritchie *

Materials Sciences Division, Lawrence Berkeley National Laboratory, University of California, Berkeley, CA 94720, USA
Department of Materials Science and Engineering, University of California, Berkeley, CA 94720, USA

Abstract

Two major mechanisms that could potentially be responsible for toughening in mineralized tissues, such as bone and dentin, have been identified—microcracking and crack bridging. While evidence has been reported for both mechanisms, there has been no consensus thus far on which mechanism plays the dominant role in toughening these materials. In the present study, we seek to present definitive experimental evidence supporting crack bridging, rather than microcracking, as the most significant mechanism of toughening in cortical bone and dentin. In vitro fracture toughness experiments were conducted to measure the variation of the fracture resistance with crack extension [resistance–curve (R-curve) behavior] for both materials with special attention paid to changes in the sample compliance. Because these two toughening mechanisms induce opposite effects on the sample compliance, such experiments allow for the definitive determination of the dominant toughening mechanism, which in the present study was found to be crack bridging for microstructurally large crack sizes. The results of this work are of relevance from the perspective of developing a micromechanistic framework for understanding fracture behavior of mineralized tissue and in predicting failure in vivo.
© 2004 Elsevier Inc. All rights reserved.

Keywords: Bone; Fracture; Toughening; Crack bridging; Microcracking

Introduction

There has been extensive research on the mechanical properties of mineralized tissues, especially cortical bone, over the past few decades (e.g., Refs. [4–6,15–17,19–22,25,32–34,36–39]). Of particular interest is the fracture toughness of such materials, which characterizes their resistance to incipient cracking and fracture, and the microstructural mechanisms that are the source of such resistance. This topic is currently of interest as it is now realized that bone mineral density cannot solely explain the therapeutic benefits of antiresorptive agents in treating osteoporosis [11], thereby reemphasizing the need to understand how factors other than bone mineral density control bone fracture.

In general, toughness is induced by two classes of mechanisms: intrinsic mechanisms that operate ahead of the crack tip and are the material's inherent resistance to microstructural damage and cracking, and extrinsic mechanisms that operate primarily behind the crack tip to promote a reduction in the driving force (e.g., the local stress intensity) at the crack tip (termed crack tip shielding) by such mechanisms as crack bridging or microcracking [7,26,27]. Intrinsic toughening, which is most important in ductile materials, acts to increase resistance to crack initiation. Extrinsic mechanisms, conversely, are invariably the prime source of toughening in brittle materials and composites and contribute to the crack growth toughness; specifically, they contribute to rising toughness with crack extension or rising resistance–curve (R-curve) behavior because the toughening mechanisms develop in the wake of the crack.

In mineralized tissue, rising R-curve behavior has been observed in both cortical bone [20,25,32–34] and dentin [19]; moreover, evidence based on microscopic observations has indicated that microcracks and crack bridges form during the fracture of both materials (e.g., Refs. [15,19,21,22,25,32–34]). Typically, microcracks preferentially form at the peritubular cuffs within the inelastic zone

* Corresponding author. Department of Materials Science and Engineering, 381 Hearst Mining Building, University of California, Berkeley, CA 94720-1760. Fax: +1-510-486-4881.
E-mail address: RORitchie@lbl.gov (R.O. Ritchie).

surrounding a macroscopic crack in (particularly human) dentin (e.g., Ref. [23]) and around osteons due to osteon matrix inferface debonding or osteon pullout in the bone (e.g., Ref. [5]). Crack bridging, conversely, involves the formation of unbroken regions that span the crack in the wake of the crack tip and act to resist crack opening. Such bridging in dentin and bone has been suggested to occur by unbroken individual collagen fibers and by so-called "uncracked ligaments" (spanning regions up to hundreds of micrometers in size), the latter resulting from either nonuniform extension of the crack front or where the main crack attempts to link-up with small cracks initiated ahead of the crack tip (e.g., Refs. [21,22,25]). Fig. 1 shows some typical examples of such mechanisms.

There has been little agreement to date, however, on which of these extrinsic mechanisms play the predominant role in toughening mineralized tissues. Some studies on the fracture behavior of cortical bone [32–34] have suggested that a microcrack-toughening mechanism, similar to that first modeled for ceramics by Evans and Faber [8], is responsible for the rising R-curve toughness behavior. Although the formation of microcracks in the damage zone ahead of the crack tip typically acts to lower the intrinsic toughness, extrinsic toughening can occur due to the formation of a "frontal process zone" ahead of the growing crack and the consequent formation of a microcracking zone in the crack wake. The resulting dilation and reduction in modulus that occur within this zone, if constrained by surrounding rigid material, can act to shield the crack tip and hence extrinsically toughen the material [8,13,31]. However, the mere existence of microcracks does not imply that this mechanism is active since the microcracks must be stable and constrained to provide toughening, otherwise their presence may be detrimental to the material toughness. Indeed, microcracking can lead to severe microstructural damage in a material, depending upon its distribution and the degree of constraint [14]; for example, degradation of the fracture toughness of cortical bone has been reported as a result of microcrack damage induced by cyclic fatigue loading [37].

More recently, studies involving scanning electron microscopy (SEM) and X-ray tomography of the crack wake have identified crack bridging as an important extrinsic toughening mechanism in cortical bone and dentin [19,21, 22,25]. Such bridges, which result primarily from uncracked ligaments and additionally from intact collagen fibrils
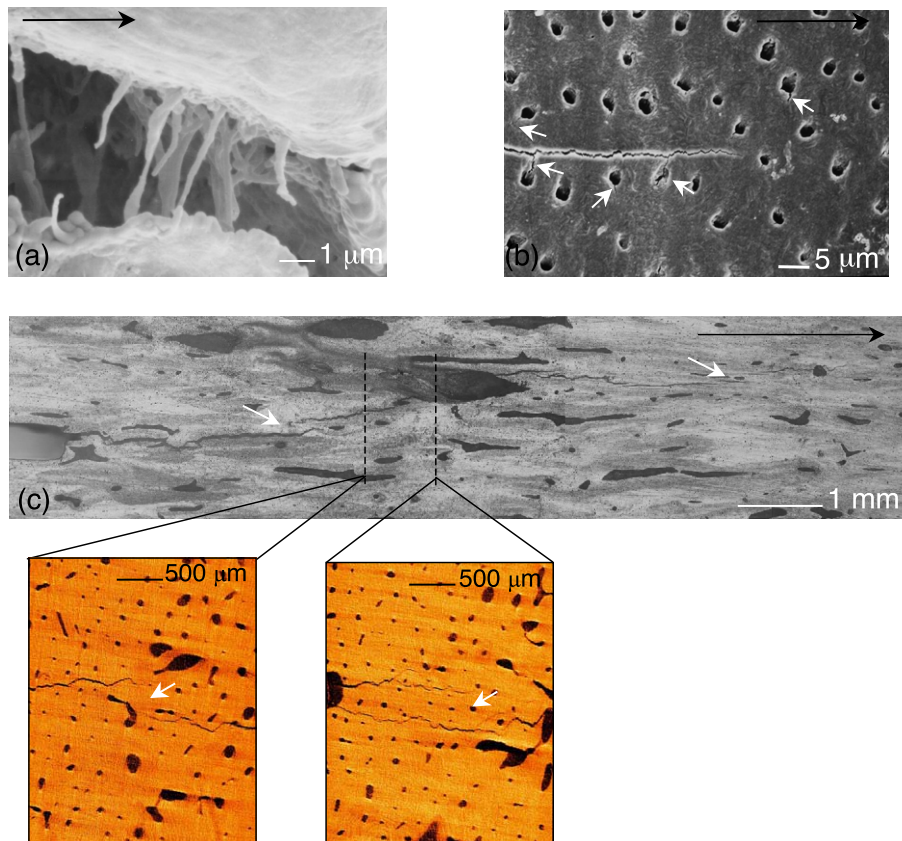

Fig. 1. Scanning electron micrographs of (a) crack bridging by collagen fibers in human cortical bone and (b) microcracking (indicated by white arrows) at tubule sites in human dentin. (c) Evidence of uncracked ligament bridging (indicated by white arrows) shown for a crack in a 61-year-old human cortical bone in an optical micrograph (top) and in X-ray computed tomographic reconstructions of through-thickness slices (Nalla RK, Kinney JH, Ritchie RO, unpublished research, 2004). The horizontal black arrow in each case indicates the direction of nominal crack growth.

[21,22,25], span the crack wake and thereby sustain a part of the applied load that would otherwise contribute to crack advance. In this way, bridging acts as an extrinsic toughening mechanism by shielding the crack tip from part of the applied driving force. As with microcracking, the mere observation of such bridges does not guarantee that they sustain load and provide toughening. While both theoretical analysis [21,22] and experimental evidence [19,22,25] have suggested that bridging provides a significant contribution to the toughness, definitive experimental proof is needed to determine whether bridging or microcracking is in fact the more important source of (extrinsic) toughness in these materials.

Measurement of the sample compliance, C, at a fixed crack size during R-curve testing provides an ideal method for determining whether bridging or microcracking is the dominant toughening mechanism. The sample compliance (inverse of stiffness) is the slope of the displacement–load curve and is commonly used to determine crack length during crack growth (e.g., R-curve) testing. Specifically, as the (major) crack length increases, the sample becomes more compliant (less stiff); for a given geometry, this change in compliance can be uniquely related to the crack length for an ideal, linear-elastic, cracked sample.

In the presence of extrinsic toughening, however, the material does not behave in an ideal manner and the compliance (for a given crack size) is affected in different ways depending on the mechanism. For the case of microcrack toughening, there is an associated reduction in elastic modulus in the microcracked region, which can be related to the volume fraction of microcracks, f_m, by [8,24]:

$$E_m/E \approx 1 - [16(1 - v_m^2)(10 - 3v_m)f_m/45(2 - v_m)], \qquad (1)$$

where E is the elastic modulus of the uncracked material, E_m and v_m are the elastic modulus and Poisson's ratio of the microcracked material, respectively, with v_m given in terms of the uncracked Poisson's ration, v, as:

$$v_m = v(1 - 16f_m/9) \qquad (2)$$

The above equations were derived using a self-consistent energy approach and apply to linear elastic solids with volume fractions of microcracks up to approximately 40% [24]. Additionally, it should be noted that in Eqs. (1) and (2), the microcrack volume fraction, f_m, is not the true volume fraction of empty space associated with the microcracks, but instead is defined as $N'(r^3)$ for penny-shaped cracks, with other definitions applying for different microcrack geometries [8,13,24]. Here N' is the total number of microcracks per unit volume and r is the mean microcrack radius. Thus, since microcracking results in a modulus decrease, there should also be a corresponding increase in sample compliance relative to the ideal case (Fig. 2). Based on published results and the present authors' observations, microcrack volume fractions surrounding a macroscopic crack are expected to be small in cortical bone and dentin,
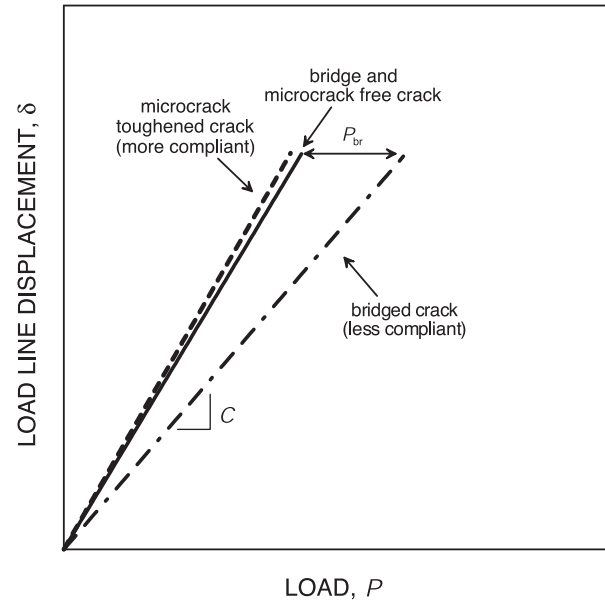

Fig. 2. Schematic illustration of the variation in compliance of a sample containing a crack of given size with the mechanism of toughening. Compared to the theoretical compliance of a linear-elastic traction-free crack, the role of crack bridging is to lower the compliance (i.e., to increase the stiffness), whereas microcracking will tend to slightly elevate the compliance (i.e., to lower stiffness).

on the order of a few percent; indeed, an upper bound estimate based on the measurements of Vashishth et al. [32] would give approximately 3% for cortical bone. For such small volume fractions, the expected modulus reduction is correspondingly small, for example, a 4% reduction in modulus results from a 3% volume fraction of microcracks. Furthermore, as this modulus reduction is limited to the microcracked zone that surrounds the crack, the effect of microcracking on the overall sample compliance is expected to be relatively minor.

In contrast, bridging in the wake of the crack serves to resist crack opening, resulting in a lower compliance (increased stiffness) than expected for the ideal case [10]. This effect on the sample compliance is typically easily measurable and forms the basis for several techniques used to analyze the role of bridging as a toughening mechanism [12,28,35]. Thus, sample compliance measurements provide an ideal method to distinguish whether microcracking or bridging is the dominant extrinsic toughening mechanism responsible for the rising R-curve behavior in mineralized tissues such as cortical bone and dentin, since an opposite effect is predicted for the two mechanisms—bridging lowers compliance whereas microcracking marginally increases it, as illustrated in Fig. 2. Accordingly, it is the objective of this paper to perform in vitro measurements of the R-curve behavior with the associated compliance analysis outlined above to determine whether crack bridging or microcracking provides the major contribution to the fracture toughness of cortical bone and dentin.

Materials and methods

Materials

Fresh frozen human cadaveric humeral cortical bone (34–41 years old) was used in this study. Compact-tension [C(T)] specimens ($n = 6$) with sample widths of W approximately 14–17 mm were machined out of blocks of bone obtained by carefully sectioning the middiaphysis section of each humerus. Notches were introduced into the C(T) specimens in the longitudinal–radial plane using a slow-speed saw and finally razor-micronotched to a root radius of ρ approximately 15 μm, where the razor micronotch was created by repeatedly sliding a razor blade over the saw-cut notch while irrigating with a 1-μm diamond slurry. The samples were oriented such that the nominal crack growth direction was along the longitudinal direction of the humerus, that is, parallel to the long axis of the osteons. Although based on expected physiological loading conditions, the transverse, and not longitudinal, cracking direction would seem to be the most relevant, it should be noted that cracks loaded such as to cause growth in the transverse direction in vitro have been found to deflect towards the longitudinal direction [3]. Accordingly, to gain a complete mechanistic understanding of the fracture of cortical bone, the present orientation would appear to be physiologically relevant, and the larger amount of crack growth that is possible in this orientation is useful experimentally.

Fractured shards of elephant tusk from an adult male elephant, *Loxodonta africana* (from the Oakland Zoo, Oakland, CA), were used for the corresponding dentin specimens. Compact-tension specimens ($n = 5$), again with W approximately 14–17 mm, were machined using similar techniques from these shards such that the dentinal tubules were oriented perpendicular to the direction of nominal crack propagation and in the plane of the crack. Further details of the specimen preparation methods are given elsewhere [19].

Resistance-curve fracture toughness testing

R-curves were measured in vitro to evaluate the resistance to fracture in terms of the stress intensity, K, as a function of crack extension, Δa, under a monotonically increasing driving force. The C(T) specimens were loaded in displacement control at a rate of approximately 0.015 mm/s using standard servohydraulic testing machines (MTS 810, MTS Systems Corp., Eden Prairie, MN) until the onset of cracking, which was determined by a drop in load, and consequent first change in compliance. The sensitivity of this detection method was verified by interrupting some tests and making direct observations of the crack extension in an optical microscope. At this point, the sample was unloaded by 10–20% of the peak load to record the sample compliance at the new crack length. This process was repeated at regular intervals until

the end of the test, at which point the compliance and loading data were analyzed to determine fracture resistance, K_R, as a function of crack extension, Δa. Crack lengths, a, were calculated from the compliance data obtained during the test using standard C(T) load line compliance calibrations [29]:

$$a/W = 1.0002 - 4.0632U + 11.242U^2 - 106.04U^3$$
$$+ 464.33U^4 - 650.68U^5 \tag{3}$$

where U is a fitting function written as:

$$U = \frac{1}{(FC)^{1/2} + 1} \tag{4}$$

where C is the sample compliance and F is a calibration constant, taken to be that which gives the best agreement between the initial compliance and crack length at the beginning of the test. Due to crack bridging, errors invariably occurred in the compliance-crack length measurements; accordingly, recalibration to the actual crack length was periodically achieved by direct measurements made using optical microscopy, with the length being measured at the crack tip ahead of the last observable "bridge." Discrepancies between the compliance and optically measured crack length were corrected by assuming that any such error accumulated linearly with crack extension. The K_R vs. Δa data obtained, in particular, the change in slope for elephant dentin, were statistically analyzed using a Student t-test.

The specimens were prepared by soaking in Hanks' Balanced Salt Solution (HBSS) in air-tight containers for at least 40 h before actual testing. Under these conditions, there was little evidence of bacterial action, and consequent bacterial degradation is believed to be negligible. The tests were conducted in ambient air (25°C, 20–40% relative humidity) with the specimens being continuously irrigated with HBSS while being tested. The sample load line compliance was determined from the slope of the displacement–load curve measured using a load cell (Model 1401-01, Key Transducers, Inc., Troy, MI) along with either a capacitance-based displacement gauge (Model HPT-150, Capacitec Inc., Ayer, MA) mounted to the specimen grips for the dentin samples or with a linear variable-displacement transducer (LVDT) (Model 381700-03, MTS Systems Corp.) mounted in the MTS load frame for the human bone specimens. Posttest observations of the cracks were performed for both bone and dentin samples using optical and scanning electron microscopy.

Compliance analysis

After R-curve testing, the final sample compliance was recorded and the crack length measured using optical microscopy. For an ideal, linear-elastic crack with no microcracking or bridging, the final compliance should be related

to the final crack length by the standard compliance equation for this specimen geometry [29]:

$$C = \frac{1}{F}\left(\frac{1+a/W}{1-a/W}\right)^2 (2.1630 + 12.219a/W$$
$$- 20.065(a/W)^2 - 0.9925(a/W)^3$$
$$+ 20.609(a/W)^4 - 9.9314(a/W)^5), \qquad (5)$$

where all variables have been previously defined and F is determined at the beginning of the experiment for the microcrack- and bridge-free configuration, that is, before crack extension. Eq. (5) is a standard elastic compliance calibration that is valid for isotropic and anisotropic linear elastic solids and is widely used in all fracture mechanics analyses for the compact-tension specimen geometry utilized in this study. Indeed, it has been successfully used for a wide range of materials—for example, metallic alloys, ceramics, and composites [1,2], the latter of which has a significant degree of mechanical anisotropy, akin to dentin and bone. The ideal (theoretical) compliance may be thus calculated using Eq. (5) and then compared to the measured compliance at the end of the R-curve test for each sample. As noted above, if the measured compliance is slightly higher or similar to the theoretical compliance, this would be consistent with the notion of microcracking as the dominant toughening mechanism; conversely, if the measured compliance is significantly lower than the theoretical value, this would confirm that bridging is the dominant toughening mechanism.

Results and discussion

Resistance-curve behavior

Load-displacement data were analyzed to evaluate the resistance to fracture in terms of the stress intensity, K, as a function of crack extension, Δa; the resulting R-curves for hydrated cortical bone and dentin are shown in Fig. 3. Cracks can be seen to grow subcritically between 4 and 7 mm before the conclusion of the test. In the case of bone, the average crack-initiation toughness, K_o, was 2.06 ± 0.2 MPa$\sqrt{\text{m}}$; the R-curves can be seen to be monotonically rising (slope = 0.39 ± 0.09 MPa$\sqrt{\text{m}}$/mm). These data agree reasonably well with the results of Vashishth et al. [32] for human cortical bone tested in the same orientation. For dentin, K_o of 1.88 ± 0.40 MPa$\sqrt{\text{m}}$ was obtained, with an initially steep slope (0.54 ± 0.16 MPa$\sqrt{\text{m}}$/mm) followed by a statistically significant [$t(8)$ = 6.709, $P < 0.05$] "plateau" region (slope of 0.06 ± 0.04 MPa$\sqrt{\text{m}}$/mm), where the toughness remained essentially constant with crack extension. Thus, the cortical bone showed a linearly rising resistance curve, whereas hydrated dentin showed rising behavior initially, followed by a plateau at larger crack extensions. The latter behav-

ior has been attributed to the larger crack-opening displacements associated with hydration in dentin (R-curves in dehydrated dentin look similar to those in bone); this issue is discussed in detail elsewhere [19].

Because the crack extends in a stable manner during R-curve testing, specimens typically did not completely fracture and it was possible to examine for relevant extrinsic toughening mechanisms in the crack wake using microscopy after R-curve testing. As shown in Fig. 1, there was visual evidence of a number of mechanisms of toughening in both dentin and bone. To provide experimental verification of the effectiveness of these mechanisms, measurements of the elastic compliance (inverse stiffness) of cracked specimens were compared to the theoretically calculated compliance of ideal, bridge- and microcrack-free, cracks of the same length using Eq. (5). Results for representative cracks in hydrated bone and dentin are shown in Fig. 4. It is apparent that the measured compliance is significantly lower than the theoretical compliance for both cases, which lends strong support to the notion that the observed bridges indeed sustain a part of the applied load, thereby providing additional resistance to crack opening and significant toughening. However, such a result does not rule out that both bridging and microcracking make significant contributions to the crack-growth toughness, and accordingly a quantitative assessment is needed (as described below). Indeed, even if there were some reduction in the stiffness from microcracking, the increase in stiffness due to bridging would more than compensate for it.

The notion that bridging dominates the toughening behavior, however, agrees well with theoretical estimates of toughening contributions based on existing models. Based on accepted models for microcrack toughening by dilatation and modulus reduction, the increase in toughness due to microcracks may be expressed as [8,13,31]:

$$K_m = 0.22\varepsilon_m E' f_m \sqrt{l_m} + \beta f_m K_c, \qquad (6)$$

where ε_m is the residual volumetric strain, E' is the plane strain elastic modulus, f_m is the volume fraction of microcracks (defined in Introduction), l_m is the height of the microcrack zone, β is a factor dependent on Poisson's ratio (approximately 1.2 [31]), and K_c is the intrinsic material toughness in the absence of microcracks. For the residual volumetric strain, the upper value of the typical range seen in ceramics (as calculated from data reported in Ref. [31]), $\varepsilon_m = 0.002$, was used. Note, this value will serve to overestimate the toughening since ε_m is directly proportional to the residual stresses in the material, which can be hundreds of MPa in ceramics, that is, values much higher than could be sustained in bone or dentin. For this model (i.e., Eq. (6)), to predict the levels of extrinsic toughening seen in Fig. 3, for example, 0.5–1 MPa$\sqrt{\text{m}}$ for dentin and 1.5–3 MPa$\sqrt{\text{m}}$ for human cortical bone, microcrack volume fractions, f_m, of approximately 25–65% in dentin and approximately 60–90% in bone would be needed, respec-
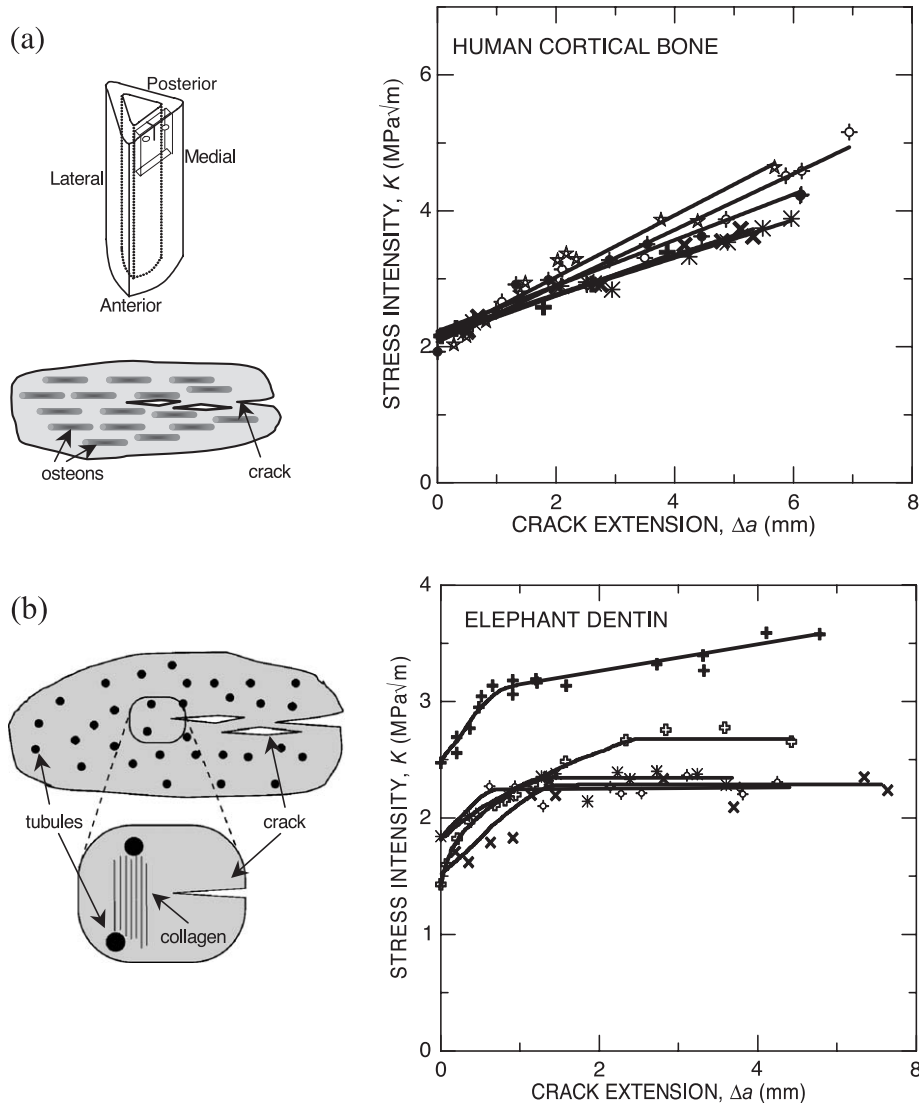
Fig. 3. $K_R(\Delta a)$ resistance-curves for hydrated (a) human cortical bone, and (b) elephant dentin in HBSS. Note the rising R-curve behavior in both cases, indicative of the active presence of extrinsic toughening mechanisms in the crack wake. The schematics on the left in (a) show the anatomical location (top) and the orientation with respect to the osteons (bottom) for cortical bone, while the schematics on the left in (b) show the orientation with respect to the tubules (top) and the collagen fibers (bottom).

tively, even though the toughening contribution was intentionally overestimated through the choice of ε_m. These are extremely high levels of microcracking that are not observed in either material; indeed, in the present study, very few microcracks at all were observed in the elephant dentin.

Recent measurements in human cortical bone by Vashishth et al. [32] report increases in microcrack densities from 2.04–2.3 (SD 0.97–0.62) to 11.1 (SD = 1.83) microcracks/mm² during R-curve tests; these authors attribute such microcracking as the mechanism of toughening in bone. The corresponding post-R-curve microcrack volume fractions can be estimated to be approximately 3% by assuming that all the microcracks are penny-shaped cracks of 175 μm diameter (midrange of the 100- to 250-μm cutoff size range used in that study). Such microcrack volume fractions of approximately 3%, as estimated from the

measurements of Vashishth et al. [32], are substantially lower than those required to produce the level of toughening that they observe experimentally and do not explain the present compliance observations (Fig. 4a). Thus, while there is clearly a definite increase in the microcrack density with crack propagation, it is totally insufficient to develop the magnitude of toughening observed in cortical bone based on existing models of microcrack toughening. It might be noted that Vashishth et al. [32] ignore all microcracks below 100 μm; however, inclusion of such microcracks would still be insufficient to explain the observed toughening.

Conversely, estimates can be made from the results shown in Fig. 4 as to the significance of bridging as a toughening mechanism. The additional load sustained at the load line, P_{br} (Fig. 2), can be used to roughly estimate the bridging contribution to the toughness, K_{br}, by assum-
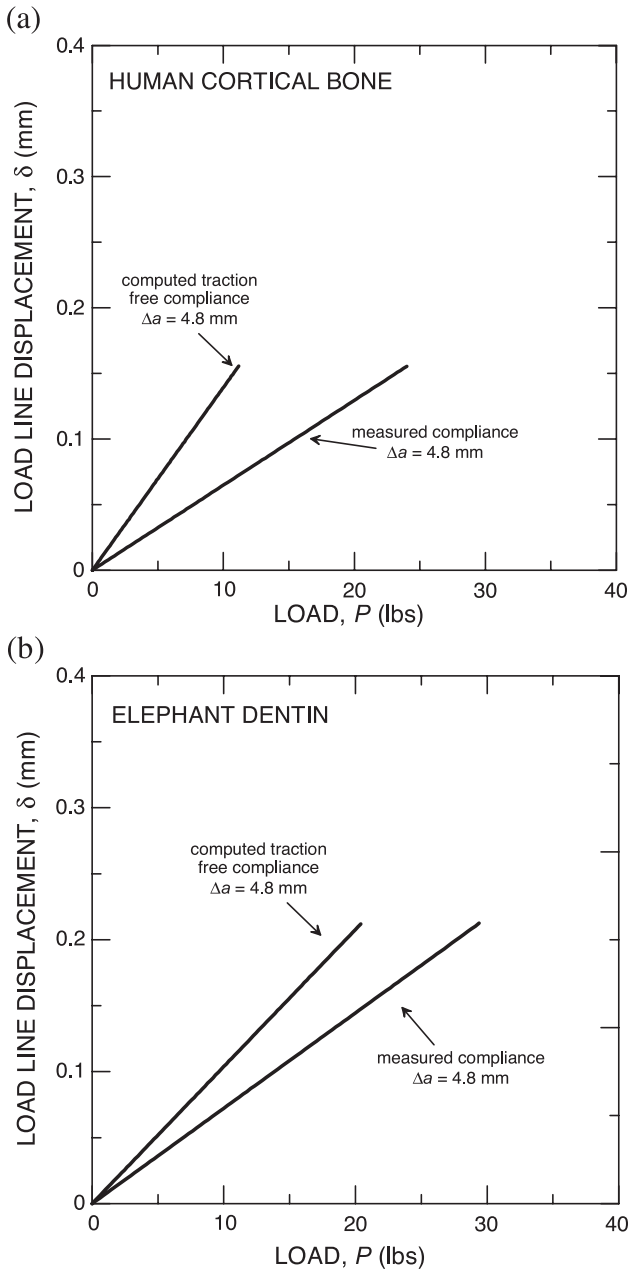
(a)

(b)

Fig. 4. Comparison of the experimental (measured) and theoretical (bridge- and microcrack-free) compliance curves for a crack of constant size in (a) human cortical bone and (b) elephant dentin. Note that in each case, the measured compliance is distinctly lower than the bridge- and microcrack-free compliance, which provides strong evidence of the role of crack bridging, as opposed to microcracking, in the toughening of these mineralized tissue materials.

ing P_{br} is applied at the load line and computing K_{br} based on the standard C(T) stress-intensity solution [28]. Such a method is not strictly accurate since it does not consider that the measured P_{br} is actually the result of bridging stresses, σ_{br}, distributed along the crack wake; however, it can provide a reasonable first approximation. In fact, previous studies have found this method to underestimate the bridging contribution, K_{br}, suggesting that such esti-

mates are conservative [18]. Applying this method to the results in Fig. 4 gives $K_{br} \approx 1$ MPa$\sqrt{m}$ for dentin and $K_{br} \approx 2$ MPa$\sqrt{m}$ for cortical bone. Since the measured toughness can be considered as the sum of the crack initiation and bridging stress intensities, that is, $K_c = K_o + K_{br}$, these estimates are entirely consistent with the degree of toughening observed in Fig. 3. We thus conclude that these results provide convincing quantitative evidence that, despite claims to the contrary [32–34], crack bridging is the dominant toughening mechanism in cortical bone; moreover, the results provide similar quantitative evidence for dentin. These conclusions are consistent with previous reports [19,22,25]. Accordingly, it would appear that the toughening effects of microcracking in these mineralized tissue materials are secondary.

Finally, because the compliance measurements presented are insensitive to the type of bridging, these results alone cannot delineate whether the toughening from bridging is a result of the observed uncracked ligaments or bridging collagen fibers. Qualitative evidence supporting uncracked ligament bridging as the main contributor may be ascertained from the fact that the toughness continues to rise over the scale of millimeters, indeed many millimeters in the case of cortical bone (Fig. 3a). The observation of bridging collagen fibers is typically limited to within tens of micrometers of the crack tip, and although this may be an important source of toughening in the presence of small cracks, collagen fibers could not possibly continue to contribute to rising toughness after several millimeters of crack extension, as seen in Fig. 3. To provide more quantitative evidence supporting this, one may apply the uniform traction Dugdale zone model of Evans and McMeeking [9] to obtain estimates of the toughening contribution from such collagen fiber bridging for cortical bone, viz.:

$$K_b^f = 2\sigma_b f_f (2l_f/\pi)^{1/2}, \tag{7}$$

where σ_b is the normal bridging stress on the fibrils (assumed to be approximately 100 MPa), f_f is the effective area fraction of the collagen fibrils active on the crack plane (approximately 0.15 from crack path observations), and l_f is the bridging zone length (approximately 10 μm from crack path observations). Using these estimates of the parameters in Eq. (7), a value of $K_b^f \approx 0.08$ MPa$\sqrt{m}$ can be obtained; similar calculations for dentin have yielded values of $K_b^f < 0.10$ MPa$\sqrt{m}$. Based on these estimates, the effect of collagen fiber bridging appears to be minimal on the macroscopic R-curve toughening. However, it should be noted here that the contribution from collagen bridging would be expected to be more significant for individual microcracks, where due to the substantially smaller size scales collagen bridges would be able to span a large percentage of the crack length.

In comparison, a limiting crack-opening displacement approach [30] can be used to estimate the corresponding

contribution from uncracked ligament bridging, K_b^{ul}, to the toughness of cortical bone:

$$K_b^{ul} = -f_{ul}K_I[(1 + l_{ul}/rb)^{1/2} - 1]$$
$$/[1 - f_{ul} + f_{ul}(1 + l_{ul}/rb)^{1/2}], \tag{8}$$

where f_{ul} is the area fraction of bridging ligaments on the crack plane (approximately 0.45 from crack path observations), K_I is the applied (far-field) stress intensity (4.5 MPa $\sqrt{m}$), l_{ul} is the bridging zone size (approximately 5 mm from crack path observations), r is a rotational factor (0.195–0.470 [30]), and b is the length of the remaining uncracked region ahead of the crack. Again, substituting typical values for these parameters, toughening of the order of $K_b^{ul} \approx 1-1.6$ MPa$\sqrt{m}$ can be expected. Similarly, values of $K_b^{ul} \approx 1-1.45$ MPa$\sqrt{m}$ have been previously reported for hydrated dentin [19]. Clearly, estimates from these models suggest that uncracked ligament bridging provides a far more significant contribution to the toughening of both cortical bone and dentin, as compared to collagen fiber bridging.

Thus, based on experimental evidence and theoretical estimates, it is clear that the primary source of bridging can be ascribed to the much larger uncracked ligaments, and that this mechanism provides the main source of fracture toughness in cortical bone and dentin.

Conclusions

Based on an experimental study of the in vitro fracture behavior of both cortical bone and dentin, the following conclusions can be made:

1. Rising R-curve fracture toughness behavior was observed in both human cortical bone and elephant dentin, indicating that extrinsic toughening mechanisms are active in the crack wake.
2. Direct observations of crack paths revealed several potential extrinsic toughening mechanisms, including crack bridging due to uncracked ligaments and collagen fibers and (in bone) zones of enhanced microcracking.
3. Compliance measurements showed that after R-curve testing, the specimens had substantially lower compliance than expected for an ideal (bridge-free) crack. Because crack bridging should decrease the measured compliance (i.e., increase stiffness) whereas microcracking should marginally increase the compliance (decrease stiffness), crack bridging is deduced to be the dominant toughening mechanism. Additionally, quantitative estimates of the contribution of bridging to the fracture toughness were in agreement with that observed in R-curve experiments.
4. Effects of microcracking on the toughness were found to be secondary. The limited role of microcracking in

toughening bone and dentin is in agreement with theoretical model-based estimates of the toughening contribution based on observed microcrack densities.
5. Because the extent of the measured R-curves (rising toughness with crack extension) continues over dimensions far larger than the scale of the observed collagen fiber bridging, uncracked ligament bridging is deemed to be the predominant toughening mechanism in these mineralized tissues for macroscopic crack propagation. This result is again consistent with theoretical model-based estimates for toughening contributions in these materials.

References

[1] ASTM E561-98. Annual Book of ASTM Standards, Vol. 03.01: metals- mechanical testing; elevated and low-temperature tests; metallography. West Conshohocken (PA): ASTM; 2002. p. 534–46.
[2] ASTM E647-00. Annual Book of ASTM Standards, Vol. 03.01: metals- mechanical testing; elevated and low-temperature tests; metallography. West Conshohocken (PA): ASTM; 2002. p. 595–635.
[3] Behiri JC, Bonfield W. Orientation dependence of the fracture mechanics of cortical bone. J Biomech 1989;22:863–72.
[4] Burstein A, Reilly D, Martens M. Aging of bone tissue mechanical properties. J Bone Jt Surg 1976;58A:82–6.
[5] Carter D, Hayes WC. Compact bone fatigue damage: a microscopic examination. Clin Orthop 1977;127:265–74.
[6] Currey JD. The mechanical properties of bone. Clin Orthop 1970; 73:209–31.
[7] Evans AG. Perspective on the development of high toughness ceramics. J Am Ceram Soc 1990;73:187–206.
[8] Evans AG, Faber KT. Crack-growth resistance of microcracking brittle materials. J Am Ceram Soc 1984;67:255–60.
[9] Evans AG, McMeeking RM. On the toughening of ceramics by strong reinforcements. Acta Metall 1986;34:2435–41.
[10] Fett T. Influence of bridging stresses on specimen compliances. J Mater Sci Lett 1991;10:1211–6.
[11] Heaney R. Is the paradigm shifting? Bone 2003;33:457–65.
[12] Hu X-Z, Mai Y-W. General method for determination of crack-interface bridging stresses. J Mater Sci 1992;27:3502–10.

[13] Hutchinson JW. Crack tip shielding by micro-cracking in brittle solids. Acta Metall 1987;35:1605–19.

[14] Kachanov M, Montagut E, Laures J. Mechanics of crack–microcrack interactions. Mech Mater 1990;10:59–71.

[15] Kahler B, Swain MV, Moule A. Fracture-toughening mechanisms responsible for differences in work of fracture of hydrated and dehydrated dentine. J Biomech 2003;36:229–37.

[16] Katz JL. The structure and biomechanics of bone. Symp Soc Exp Biol 1980;34:137–68.

[17] Keaveny TM, Bartel DL. Effects of porous coating and collar support on early load transfer for a cementless hip prosthesis. J Biomech 1993;26:1205–16.

[18] Kruzic JJ, Cannon RM, Ritchie RO. Crack size effects on cyclic and monotonic crack growth in polycrystalline alumina: quantification of the role of grain bridging. J Am Ceram Soc 2004;87: 93–105.

[19] Kruzic JJ, Nalla RK, Kinney JH, Ritchie RO. Crack blunting, crack bridging and resistance-curve fracture mechanics in dentin: effect of hydration. Biomaterials 2003;24:5209–21.

[20] Malik CL, Stover SM, Martin RB, Gibeling JC. Equine cortical bone exhibits rising R-curve fracture mechanics. J Biomech 2003;36:191–8.

[21] Nalla RK, Kinney JH, Ritchie RO. Effect of orientation on the in vitro fracture toughness of dentin: the role of toughening mechanisms. Biomaterials 2003;24:3955–68.

[22] Nalla RK, Kinney JH, Ritchie RO. Mechanistic fracture criteria for the failure of human cortical bone. Nat Mater 2003;2:164–8.

[23] Nalla RK, Kinney JH, Ritchie RO. On the fracture of human dentin: is it stress- or strain-controlled? J Biomed Mater Res 2003;67A: 484–95.

[24] O'Connell RJ, Budiansky B. Seismic velocities in dry and saturated cracked solids. J Geophys Res 1974;79:5412–26.

[25] Pezzotti G, Sakakura S. Study of the toughening mechanisms in bone and biomimetic hydroxyapatite materials using Raman microprobe spectroscopy. J Biomed Mater Res 2003;65A:229–236.

[26] Ritchie RO. Mechanisms of fatigue crack propagation in metals, ceramics and composites: role of crack-tip shielding. Mater Sci Eng 1988;103:15–28.

[27] Ritchie RO. Mechanisms of fatigue-crack propagation in ductile and brittle solids. Int J Fract 1999;100:55–83.

[28] Ritchie RO, Yu W, Bucci RJ. Fatigue crack propagation in ARALL laminates: measurement of the effect of crack-tip shielding from crack bridging. Eng Fract Mech 1989;32:361–77.

[29] Saxena A, Hudak Jr SJ. Review and extension of compliance information for common crack growth specimens. Int J Fract 1978; 14:453–68.

[30] Shang JK, Ritchie RO. Crack bridging by uncracked ligaments during fatigue-crack growth in SiC-reinforced aluminum-alloy composites. Metall Trans A 1989;20A:897–908.

[31] Sigl LS. Microcrack toughening in brittle materials containing weak and strong interfaces. Acta Mater 1996;44:3599–609.

[32] Vashishth D, Behiri JC, Bonfield W. Crack growth resistance in cortical bone: Concept of microcrack toughening. J Biomech 1997;30: 763–9.

[33] Vashishth D, Tanner KE, Bonfield W. Contribution, development and morphology of microcracking in cortical bone during crack propagation. J Biomech 2000;33:1169–74.

[34] Vashishth D, Tanner KE, Bonfield W. Experimental validation of a microcracking-based toughening mechanism for cortical bone. J Biomech 2003;36:121–4.

[35] Wittmann FH, Hu X. Fracture process zone in cementitious materials. Int J Fract 1991;51:3–18.

[36] Wright T, Hayes W. The fracture mechanics of fatigue crack propagation in compact bone. J Biomed Mater Res 1976;7(10):637–48.

[37] Yeni YN, Fyhrie DP. Fatigue damage-fracture mechanics interaction in cortical bone. Bone 2002;30:509–14.

[38] Yeni YN, Fyhrie DP. A rate-dependent microcrack-bridging model that can explain the strain rate dependency of cortical bone apparent yield strength. J Biomech 2003;36:1343–53.

[39] Zioupos P, Currey JD. Changes in the stiffness, strength, and toughness of human cortical bone with age. Bone 1998;22:57–66.